Single-Molecule Morphology of Topologically Digested Olympic Networks

Saminathan Ramakrishnan,[1] Zihao Chen,[2] Yair Augusto Gutierrez Fosado,[1] Luca Tubiana,[3,4] Willem Vanderlinden,[1] Nicholas Jon Savill,[2] Achim Schnaufer,[2] and Davide Michieletto[1,5]

[1]*School of Physics and Astronomy, University of Edinburgh, Peter Guthrie Tait Road, Edinburgh EH9 3FD, United Kingdom*
[2]*Institute of Immunology & Infection Research, University of Edinburgh, Ashworth Laboratories, Charlotte Auerbach Road, Edinburgh EH9 3FL, United Kingdom*
[3]*Physics Department, University of Trento, via Sommarive, 14 I-38123 Trento, Italy*
[4]*INFN-TIFPA, Trento Institute for Fundamental Physics and Applications, I-38123 Trento, Italy*
[5]*MRC Human Genetics Unit, Institute of Genetics and Cancer, University of Edinburgh, Edinburgh EH4 2XU, United Kingdom*

(Received 1 November 2023; accepted 23 January 2024; published 20 February 2024)

The kinetoplast DNA (kDNA) is the archetype of a two-dimensional Olympic network, composed of thousands of DNA minicircles and found in the mitochondrion of certain parasites. The evolution, replication, and self-assembly of this structure are fascinating open questions in biology that can also inform us how to realize synthetic Olympic networks *in vitro*. To obtain a deeper understanding of the structure and assembly of kDNA networks, we sequenced the *Crithidia fasciculata* kDNA genome and performed high-resolution atomic force microscopy and analysis of kDNA networks that had been partially digested by selected restriction enzymes. We discovered that these topological perturbations lead to networks with significantly different geometrical features and morphologies with respect to the unperturbed kDNA, and that these changes are strongly dependent on the class of DNA circles targeted by the restriction enzymes. Specifically, cleaving maxicircles leads to a dramatic reduction in network size once adsorbed onto the surface, while cleaving both maxicircles and a minor class of minicircles yields noncircular and deformed structures. We argue that our results are a consequence of a precise positioning of the maxicircles at the boundary of the network, and we discuss our findings in the context of kDNA biogenesis, design of artificial Olympic networks, and detection of *in vivo* perturbations.

DOI: 10.1103/PRXLife.2.013009

I. INTRODUCTION

The mitochondrial genome of *Kinetoplastid* parasites displays one of the most unique and complex topologies in nature [1–7]. The so-called "kinetoplast DNA" (i.e., associated with the cellular body, or "plastos," near the parasite flagellum that give it its movement, or "kinetikos") is a unique genome with a complex topology. In the organism *Crithidia fasciculata*, it is formed by around 5000 interlinked DNA minicircles (2.5 kb) and around 30 larger DNA maxicircles (30 kb). The DNA rings are assembled and replicated into a two-dimensional (2D) network and contained in a membraneless DNA-dense region of $1\ \mu m \times 0.4\ \mu m$ within the mitochondrion. The maxicircles mostly encode rRNAs and mRNAs for oxidative phosphorylation and mitoribosomes, while the minicircles encode guide RNA genes required for posttranscriptional editing of the mRNAs [1,8,9]. Kinetoplast DNA replication and biogenesis are not fully understood and are topics of intense debate in the parasitology community [4,10–16].

There are several open questions in the field of trypanosome and kinetoplastid biology; for instance, it is unclear (1) how kDNA was evolutionally preferred over other simpler forms of genomes (e.g., longer DNA rings, as in human mitochondria) and (2) whether each genetic class of rings (e.g., maxicircles and minicircles) occupy specific and distinct positions within the kDNA structure or whether they are uniformly and randomly dispersed [17]. Interestingly, a strain of *Trypanosome brucei* can be evolved—under certain conditions—to survive and replicate without kDNA [13,18]. Overall, there are a number of unanswered questions about the evolutionary advantage of this structure and whether it is limited to a specific life stage of the parasite.

Recently, the bio- and polymer physics community used *C. fasciculata* kDNA as archetype of a 2D polymer, which is otherwise challenging to realize synthetically [19–22]. In general, the polymer physics of networks of interlinked rings, be it one-, two-, or three-dimensional (1D, 2D, and 3D, respectively), have not been studied thoroughly mainly because of experimental challenges [23,24]. Thus, it remains rather overlooked how the topology of so-called "Olympic" networks affects their material properties, although preliminary works suggest that they may display unique features, such as strong nonlinear stress response [25,26], weaker swelling [27,28], percolation [29–31], and active elastic tuning [32,33]. Linking this back to the biogenesis of kDNA in *Kinetoplastids*, it remains to be determined which—if any—of these properties are required for the biological functions of kDNA in the cell.

Simulations of polymer rings with tunable linking degree suggest that a mean linking degree, or valence, of 3—similar to that found in kDNA structures [34–36]—may reflect the fact that these networks are poised at the percolation point,

where a random graph starts displaying a system-spanning component [30,31,37]. In fact, a random graph with valence 3 is optimally connected, i.e., it displays percolation but without redundant links between circles, thus ensuring integrity of the structure while optimizing the rate of replication, which in *C. fasciculata* occurs through decatenation of minicircles from the network [4,31]. At the same time, while the material and elastic properties of kDNA networks are still largely unknown, recent work has estimated the bending stiffness to be in the range of $\kappa \simeq 10^{-21}$–10^{-19} J [21,36] and in-plane Young modulus $Y \simeq 0.1$ pN/μm [36]. Since the elasticity of an Olympic network correlates with the mean linking number [25,37,38], we expect that the kDNA elasticity will strongly depend on its underlying topology.

To achieve a better understanding of the connection between material properties and underlying topology, precise single-molecule measurements of experimental Olympic structures are needed. To date, the only synthetic Olympic structures were 1D polycatenanes [26,39,40] and bulk 3D Olympic gels [32,33], the latter made from DNA plasmids and type 2 topoisomerase. Despite these recent advances in the synthesis of catenated structures, there is no experimental method that can precisely quantify the topology of an Olympic network (especially 3D ones). Qualitative single-molecule characterization of kDNA networks have been performed using electron microscopy [2,41,42] and more recently atomic force microscopy (AFM) [43,44].

In our most recent AFM study [36] we performed quantitative image analysis and discovered that AFM, coupled to molecular dynamics simulations, can provide insights into the topology of Olympic networks at single-molecule resolution. In this work, we use AFM, quantitative image analysis, and polymer theory to understand more about the structure of kDNA and Olympic networks in general. Specifically, by exploiting the fact that catenated DNA circles can be cleaved by sequence-specific restriction enzymes, we perturb the topology of the network and measure the changes in network morphology. While topological perturbations to kDNA have been explored in the literature (see Refs. [22,34,45]), existing works have not quantitatively measured changes in network morphologies. More specifically, (1) Cozzarelli and coauthors were able to correctly determine the average valence of *C. fasciculata* kDNA by progressively linearizing some of its minicircles with XhoI restriction enzyme [34]; (2) Yadav and coauthors measured the shape autocorrelation, and hence the relaxation properties, of networks that had been treated with different restriction enzymes via imaging and discovered that more digested structures had a longer relaxation time, in line with a reduction in network connectivity [22]; and (3) Ragotskie and coauthors caused light-induced nonspecific damage to *C. fasciculata* kDNA and observed the persistence of a 1D edge loop, consistent with the estimation that the kDNA border is at least fourfold redundantly linked with respect to the inner minicircles [45]. In our work we wanted to complement these studies and provide a single-molecule view of kDNA networks that underwent specific topological perturbations.

To achieve *accurate* and *specific* topological perturbations, we first deep sequenced *C. fasciculata* kDNA and discovered that it contains 18 classes of minicircles, the most abundant of these covering 85% of the network. Through the sequencing, we were able to identify specific restriction endonucleases (REs) that digest different parts of the kDNA structure. We then employed some of these REs to partially digest kDNA and discovered that, for instance, cleaving maxicircles yields significantly shrunk networks. On the contrary, cleaving both the minor class (∼10% of total) and maxicircles yields significantly larger and noncircular structures. We qualitatively explain these findings with a scaling theory, as kDNA networks with less mass ought to display weaker adsorption to the surface while less connected networks are expected to display a weaker bulk modulus and to extend more along the surface. Finally, by cleaving all, and only, minicircles we confirmed that most of the maxicircles in the kDNA are interlinked with each other. We argue that our results shed some light on this fascinating and unique structure and potentially inform assembly strategies to synthetically design 2D Olympic networks.

II. RESULTS

A. Deep sequencing of *C. fasciculata* kDNA reveals 18 classes of minicircles

Kinetoplast DNA from *C. fasciculata* was purchased from Inspiralis at 100 ng/μl in TE buffer (10 mM Tris-HCl pH 7.5, 1 mM EDTA). A sample of kDNA was sent for deep sequencing at NovoGene. We then performed *de novo* DNA assembly of 4.7 million pair-end reads (150 bp) using KOMICS [46]. We performed several quality checks, including searching for the universally conserved minicircle sequence CSB3 (GGGGTTGGTGT) and comparing our contigs with known sequences of CfC1 [47], *Trypanosoma congolense*, and *Trypanosoma brucei* [48] (see Methods). Overall, the final assembly incorporated over 96% of all the 4.7 million reads and displayed complete coverage. We detected 18 distinct classes of minicircles with less than 75% sequence identity, and their relative abundance was estimated from mean read depth calculated by SAMtools [49]. All 18 classes of minicircles have roughly the same size 2402.8 ± 68.6 nucleotides. The major class composes 85.2% of the kDNA, a first minor class 10.9%, a second minor class 1.8%, and the other classes make up about 2.1% of the kDNA [Fig. 1(a)]. Assuming that the kDNA network contained 5000 minicircles, we estimated 9 to 10 maxicircles per network [34].

C. fasciculata maxicircle genes boundaries were predicted with *Leishmania major* maxicircle annotation to extract unedited genes. We used published transcriptomic data of *C. fasciculata* from *in vitro* culture and mosquito hindguts to validate unedited maxicircle gene annotations and predict edited encrypted genes [51]. T-masked mapping using T-aligner [52] confirmed complete editing in strain CfC1 of mRNAs from at least four cryptic genes: ATPase subunit 6 (A6), ribosomal protein S12 (RPS12 or uS12m), NADH dehydrogenase subunit 7 (ND7), and cytochrome oxidase subunit 2 (COXII). Guide RNA genes were identified on 13 out of 18 minicircle classes, which captured the same gRNAs on contigs containing the annotated minicircle fragments in previous study [52]. However, no gRNA genes were found on the major and the 1st minor minicircle classes, presumably reflecting the limited

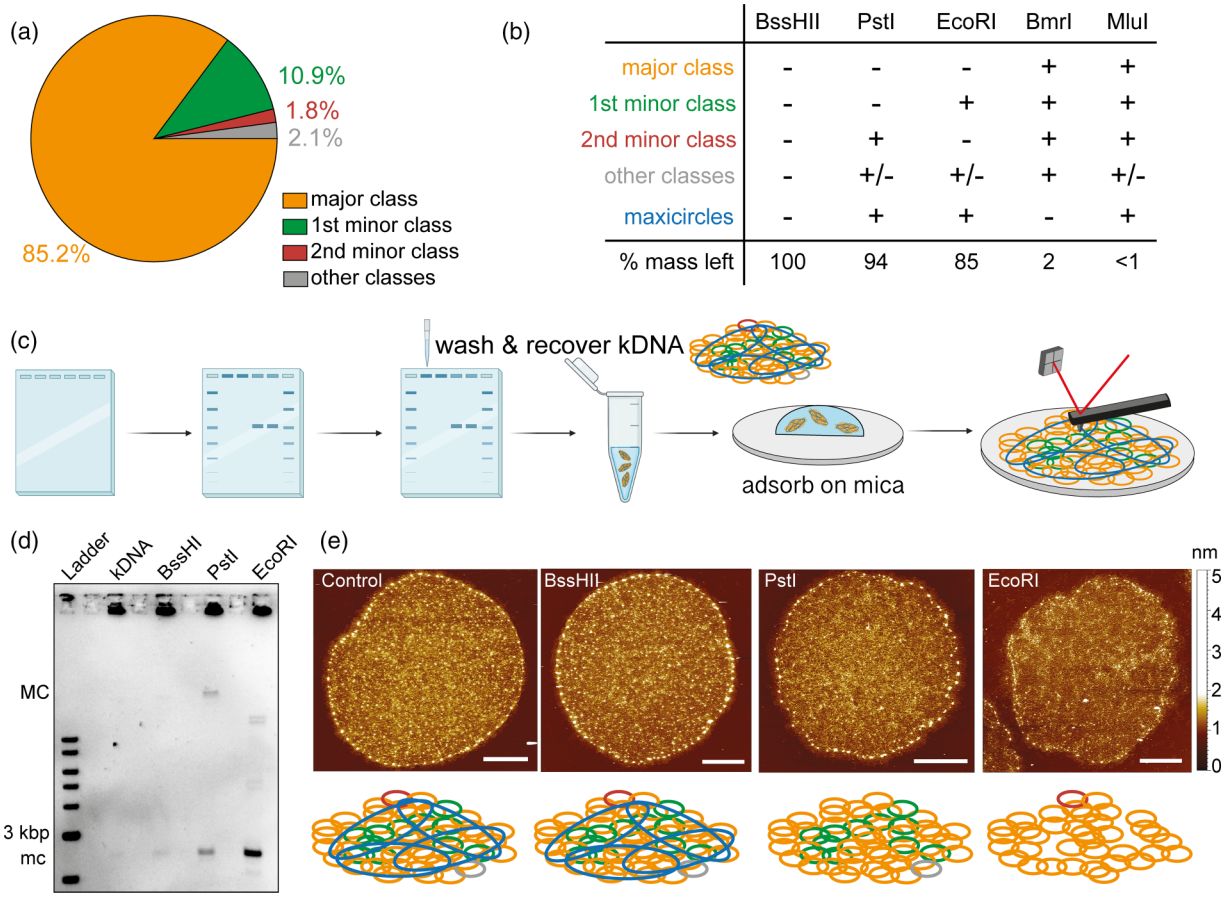

FIG. 1. (a) Minicircles relative copy number from *C. fasciculata* kDNA sequencing and assembly (see methods). (b) Table with examples of restriction enzymes that can partially digest (+) or not (−) kDNA components (see the Supplemental Material for a full table with 243 enzymes [50]). ± denotes digest of some of the "other" classes. (c) Protocol for preparation of clean samples of partially digested kDNA: we load partially digested samples in wells and run gel electrophoresis in a 1.5% agarose gel at 10 V/cm for 20 minutes. The intact and partially digested kDNA structures are too big to travel through the gel and remain stuck in the wells. We flush the wells and recover the partially intact kDNA, which are now cleaned from linearized products and enzymes. (d) Gel electrophoresis showing partially digested kDNA samples. Linearized maxicircles (MCs) run at about 30 kbp, while minicircles (mc) run at 2.5 kbp. (e) From left to right: images of undigested, BssHII-, PstI-, and EcoRI-treated samples. The height color scale is the same throughout the paper. At the bottom, we show color-coded sketches of the networks: blue, maxicircle; orange, major minicircle class; green, first minor minicircle class; red and gray, second and other minicircle classes.

number of edited sequences that could be confirmed by the available transcriptomics data.

Finally, RE cutting sites on *C. fasciculata* minicircles and maxicircle were predicted for enzymes available from New England Biolabs [see Fig. 1(b) and the Supplemental Material [50] for a full table]. Specifically, we chose BssHII as negative control, PstI as cutting maxicircles and a small <4% fraction of minicircles, EcoRI cutting maxicircles and around 13% of the minicircles, and finally BmrI, cutting all, and only, minicircles. Through these enzymes, we specifically implement topological perturbations to the kDNA structure with the aim of quantifying specific changes in their morphology via AFM.

B. Preparation of partially digested kDNA for AFM

For restriction digestion with EcoRI, PstI, and BssHII, 1 µl of enzyme (10 units) was used to digest 1 µg of kDNA in 1× rCutsmart buffer, overnight at 37 °C. The BssHII-treated sample was also incubated at 50 °C for 2 hours prior to overnight incubation at 37 °C, as per NEB recommendation. We found that during the AFM sample preparation, the mica surface was quickly covered by recombinant albumin in rCutSmart buffer and restriction digested mini and maxicircles, particularly at high magnesium concentration. Thus, enzyme-treated partially digested kDNA structures were poorly adsorbed on the mica surface. To solve this issue, we developed a methodology to remove linearized mini- and maxicircles, enzymes, and albumin for AFM sample preparation as follows [see also Fig. 1(c)]: the kDNA sample was first prestained with diluted SybrGold and ran in 1.5% agarose gel at about 10 V/cm for 20 minutes [see Figs. 1(c) and 1(d)]. The gel tray was then removed from the tank and placed on a UV transilluminator. Next 1× TE buffer in the well was gently pipetted out and replaced with 80 μl of adsorption buffer (10 mM Tris-HCl pH 7.9, 10 mM $MgCl_2$, 1 mM EDTA). This step was repeated twice and 50 µl of adsorption buffer was left in the well after the second wash. Under UV light, a fluorescent layer was visible on the wall of the well; this is

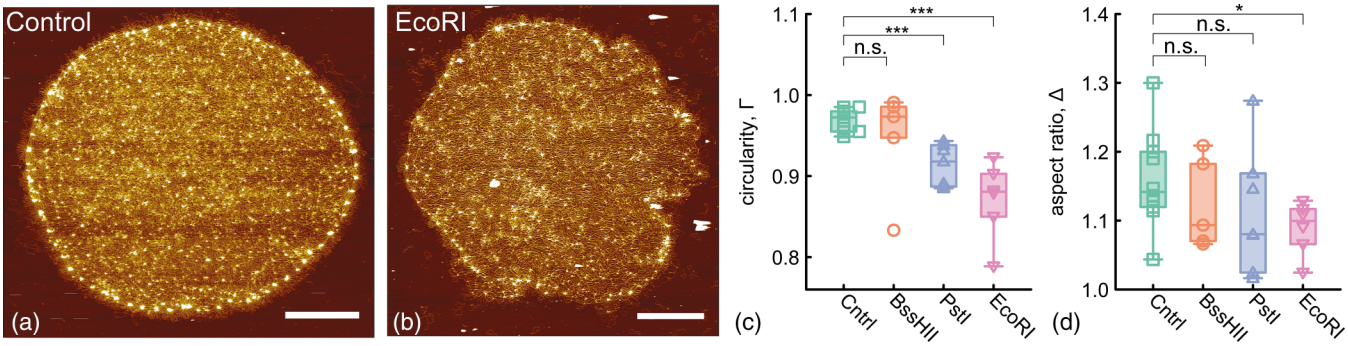

FIG. 2. (a), (b) Sample AFM images of control and EcoRI-treated samples. Scale bar is 2 μm. (c) Box plot showing the circularity Γ. Smaller $\Gamma = 4\pi(\text{area}/\text{perimeter}^2)$ indicate that the perimeter is longer than the one of a perfect circle and it quantifies irregular kDNA borders. (d) Box plot showing aspect ratio $\Delta = M/m$ between major and minor axes. Lower aspect ratios indicate shapes with more similar major and minor axes. EcoRI-digested structures display more irregular borders but the overall shape is less ellipsoidal and more circular.

because the kDNA structure contains thousands of DNA rings that can individually travel through the gel, but remain stuck in the well when linked with each other in the (partially) intact kDNA [Fig. 1(d)]. More specifically, we found that the kDNA becomes weakly adsorbed on the wall of the well and is easily removable by washing. The kDNA was either gently flushed using a pipette with 10–20 μl of adsorption buffer or gently touched with a pipette tip to resuspend the kDNA back into the buffer. We took utmost care to avoid disrupting kDNA integrity at this stage. After resuspension, a 50 μl of sample was recovered and adsorbed on freshly cleaved mica for 10 minutes. The sample was dip washed in ultra-pure water for 1 minute and gently air dried in ultrapure nitrogen stream [see Fig. 1(e) and the Supplemental Material [50] for sample images)].

C. Partially digested structures display irregular borders

First, we noticed that EcoRI-treated networks (missing all maxicircles and around 13% of minicircles) appeared structurally disrupted, while the others were, in first approximation, largely unperturbed [Fig. 1(e)]. To quantify this change in morphology we measured the circularity Γ and aspect ratio Δ (see Fig. 2). To obtain these two quantities, we manually traced the closed contour of the kDNA structures in ImageJ, and computed the circularity as $\Gamma = 4\pi(A/p^2)$, where A is the area of the closed curve and p its perimeter, while the aspect ratio as $\Delta = M/m$ where M and m are the major and minor axes of a fitted ellipse. A value of $\Gamma = 1$ indicates that the perimeter is that of a perfect circle, while $\Gamma < 1$ indicates longer, typically irregular, perimeters. At the same time, Δ refers to the shape of the overall object, with $\Delta = 1$ indicating an object with near circular symmetry, and $\Delta > 1$ an ellipsoidal object (and a rod in the limit $\Delta \to \infty$).

As shown in Fig. 2(c), we observe a significant (P value < 0.001) decrease in circularity in both PstI- and EcoRI-treated samples, but no significant change of Γ in our BssHII control. The value of Γ drops from near 1 for the control to below 0.9 for EcoRI-treated samples, reflecting the appearance of irregular kDNA borders, almost "blebbing," visually evident in the AFM images [Figs. 2(a) and 2(b)]. Additionally, we find a decrease, albeit more modest, in the aspect ratio Δ reflecting more symmetric structures, with a smaller difference between major and minor axes [Fig. 2(d)]. This confirms that the control samples are somewhat ellipsoidal with a well-defined major axis roughly 20% longer than the minor axis.

Interestingly, the fact that PstI-treated samples show a minor change in circularity Γ suggest that they contribute to the structural integrity of the network, especially of the border. It is also interesting to note at this stage that the mass contribution of maxicircles is about 2.3%, i.e., around 200 10^3 kg/mol within a total of 8.5×10^6 kg/mol for the whole kDNA. Figure 2(c) then suggests that cleaving both maxicircles and the minor class of minicircles (in total about 15% of the kDNA mass) has a compound effect in the network morphology likely due to a decrease in network connectivity [22,34].

D. Cleaving maxicircles yields significantly shrunk networks

To understand the specific structural role of maxicircles, we decided to focus on PstI-treated kDNA structures, which lack maxicircles and a small (<4%) fraction of minicircles. First, we validated in our agarose gel that a small number of minicircles are cleaved along with maxicircles in PstI-treated samples [Fig. 1(d)]. Second, and more importantly, we observe that PstI treatment causes a dramatic reduction in kDNA area A, or diameter $d = \sqrt{A}$, from around $d = 8$ μm to around $d = 5.5$ μm, i.e., a 1.5-fold shrinkage with respect to the control and BssHII-treated samples (Fig. 3). Curiously, and unexpectedly, EcoRI-treated samples appear to recover a larger size compared with PstI-treated kDNAs [Fig. 3(c)].

We can try to rationalize this puzzling observation with a simple scaling argument: the free energy of adsorption of a soft polymeric cylinder on a surface can be written as [53]

$$\mathcal{F} = k_B T \kappa \frac{D_0^2}{D^2} - k_B T \delta f_b N, \tag{1}$$

where D is the average extension of the polymers away from the surface, κ is an effective stiffness that is proportional to the in-plane Young modulus, δ is an effective interaction between the monomers and the surface, and N is the total length of the polymers in the cylinder [see Fig. 3(d) for a schematics]. Assuming that the whole kDNA mass is confined within a layer D from the surface, the fraction of mass adsorbed is approximately $f_b \simeq a/D$, where a is the extent of the attractive

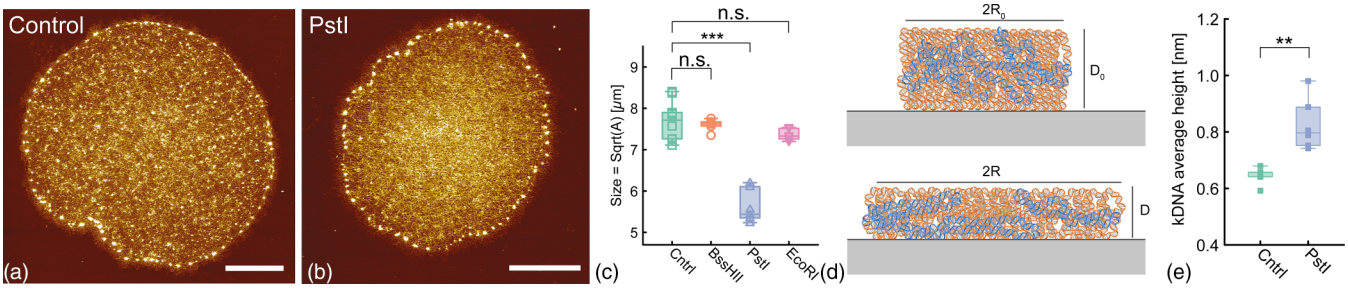

FIG. 3. (a), (b) Examples of AFM images of control and PstI-treated samples (scale bar is 2 μm). (c) Box plot of the diameter $d = \sqrt{\text{area}}$ of kDNAs. (d) Schematics sketching weak (top) and strong (bottom) adsorption of kDNA to the mica. (e) Box plot of the average median height of the kDNA structures for control and PstI-treated samples (see the Supplemental Material [50] for details).

layer from the surface. We can substitute this into Eq. (1),

$$\mathcal{F} = k_B T \kappa \frac{D_0^2}{D^2} - k_B T \delta \frac{a}{D} N, \tag{2}$$

and minimize it with respect to D, i.e., $\partial \mathcal{F}/\partial D = 0$, to obtain

$$\frac{D}{D_0} = 2 \frac{D_0}{a} \frac{\kappa}{\delta N} \sim \kappa (\delta N)^{-1}. \tag{3}$$

This equation implies that the average height of kDNA away from the adsorbing surface is inversely proportional to the effective adsorption strength δN, and directly proportional to the stiffness κ, respectively. Assuming that the whole kDNA is contained within a constant cylindrical volume $V = \pi R_0^2 D_0 = \pi R^2 D$ we obtain a relationship between the average kDNA extension R and the total adsorption energy δN scaling as

$$\frac{R}{R_0} \sim \left(\frac{\delta N}{\kappa} \right)^{1/2}, \tag{4}$$

implying that the more the kDNA mass, i.e., the larger N, the stronger the adsorption strength and the larger the planar extension R of the kDNA network. This scaling argument entails that the lack of maxicircles decreases the overall mass of kDNA, in turn decreasing the net adsorption strength of the kDNA structure. At the same time, as expected, the larger the kDNA in-plane stiffness κ, the smaller the lateral extension or spreading along the surface.

This simple scaling argument is in line with our observations: removing maxicircles, i.e., decreasing δN, reduces R, as seen in Fig. 3(c), and increases the average height, as seen in Fig. 3(e), where we compute the median kDNA height from the mica (see the Supplemental Material for details [50]). On the other hand, we note that the mass lost due to PstI treatment amounts to about 2% of the total mass (see above). Because of this, we expect a relatively small change in kDNA extension, in marked contrast with the significant (1.5-fold) reduction in kDNA diameter seen in experiments [Fig. 3(c)]. Additionally, according to Eq. (4), we should expect a similar shrinking in networks where the minor class of minicircles, accounting for about 10% of kDNA mass, has been cleaved. On the contrary, we did not observe such shrinkage in EcoRI-treated networks, which in fact displayed more extended structures [Fig. 3(c)]. These contrasting results may be reconciled by arguing that while the removal of maxicircles leads to a shrinkage of the network due to smaller adsorption strength (δN), the additional cleavage of a considerable ∼10% fraction of minicircles reduces the topological connectivity and the in-plane stiffness (κ) of the network, in turn allowing easier spreading on the surface.

E. EcoRI-treated networks display significantly disrupted hubs

After having quantified global changes to kDNA morphology, we then turned our focus to smaller-scale substructures. More specifically, from the AFM images we realized that the hubs, or rosette, structures that characterize intact kDNA are affected by partial digestion. In Figs. 4(a)–4(d) we show representative zoomed-in sections of kDNAs, showing a series of hubs at the periphery of partially digested kDNAs. To quantify their state, we extract the height of the tallest pixel across several tens of hubs around each kDNA: while BssHII- and PstI-treated hubs are not significantly affected, EcoRI treatment causes a significant disruption, with the hubs' height reducing from 3.3 ± 0.7 nm to 2.6 ± 0.5 nm [P value < 0.001, Fig. 4(e)]. We note that even for the control case, the average height is smaller than the one expected for several (possibly tens) of DNA strands overlapping each other at the hub [45]—each around 2 nm thick in the hydrated DNA structure—due to (1) imaging dehydrated DNA and (2) the compression of the DNA by the AFM tip [36]. Nevertheless, the qualitative and quantitative disruption in the EcoRI-treated samples is

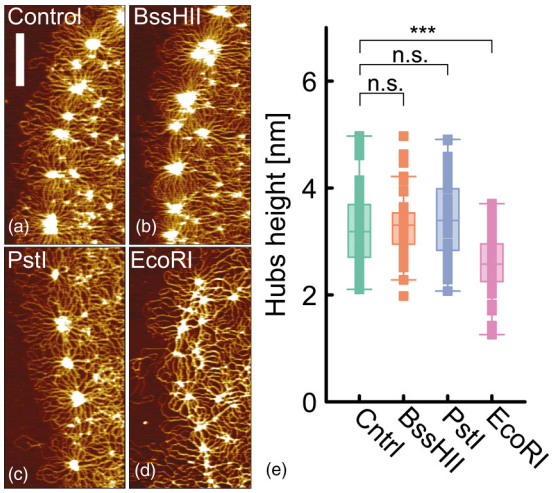

FIG. 4. (a)–(d) Sample AFM images (zoomed in at the borders) of control, BssHII, PstI, and EcoRI samples. The scale bar is 500 nm. (e) Box plot showing the height of the hubs for the different samples.

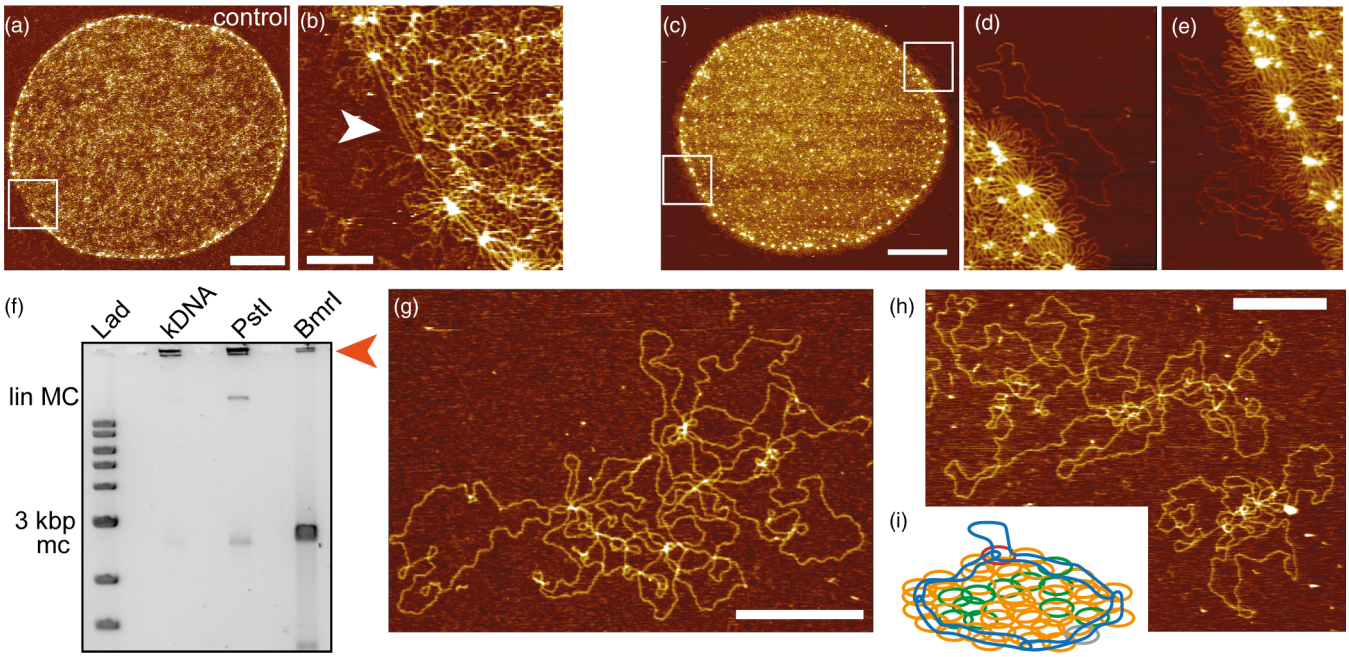

FIG. 5. (a)–(e) AFM images and zoomed in regions displaying examples of maxicircles weaved at the periphery (white arrows) and threading through minicircles and hubs (white circle). Scale bar in (a) and (c) 2 μm. Scale bar in (b) is 500 nm. The thread highlighted by the arrow is around 1.1 μm, longer than ∼400 nm that can be reached by a stretched minicircle. (f) Gel elctrophoresis comparing kDNA, PstI-treated kDNA, and BmrI-treated kDNA. The last enzyme cuts all minicircles but leaves maxicircles intact. The presence of DNA mass in the well (orange arrow) suggests that the maxicircles are linked together. (Lin MC = linearized maxicircles, mc = minicircles). (g), (h) AFM images of maxicircles purified from BmrI-treated samples and displaying linking. Scale bar is 500 nm. (i) Sketch of kDNA model with some of the maxicircles forming a sublinked network and weaving around the periphery.

clear and points to the fact that hubs are mostly made by essential crossings between minicircles rather than maxicircles. At the same time, we note that PstI-treated samples do not display significantly disrupted hubs, but do display fewer connections between the hubs [Fig. 4(c)] and also more irregular borders [Fig. 2(c)].

F. Maxicircles form an Olympic subnetwork and weave through hubs at the periphery

Our findings suggest that (1) hubs are mostly made by links between minicircles (Fig. 4) and (2) maxicircles contribute to provide structural integrity to the kDNA border (Fig. 2). While it is well known that during kDNA replication the minicircles are polymerized and reattached at the periphery of the parent kDNA by enzymes [4], the fate of maxicircles and their position within the kDNA after cell division are unknown. Still, we note that during cell division, the maxicircles form the so-called "nabelschnur," a DNA bridge connecting newly replicated kDNAs in the daughter cells [54], suggesting that they may assume a more peripheral position compared to minicircles. In light of this, and motivated by the dramatic structural and morphological change in PstI-treated samples, we hypothesized that at least some maxicircles may be weaved along the kDNA periphery and provide direct support to the border. To qualitatively test this hypothesis, we first visually inspected AFM images of nondigested samples, and observed clear signatures of maxicircles joining hubs and threading minicircles along the periphery of intact kDNAs [see white arrow in Fig. 5(a) and 5(b)], and we also identified cases in which maxicircles were clearly linked near the border of the network and spreading outside it [Figs. 5(c)–5(e)]. To further understand whether the maxicircles are themselves forming a subnetwork, we treated kDNAs with BmrI, a restriction enzyme that cuts all minicircles but leaves maxicircles intact. Intriguingly, BmrI-treated samples displayed a consistent DNA band that did not travel into the gel [Fig. 5(f)]. This suggests that maxicircles in *C. fasciculata* are linked with each other, as found in *Trypanosoma equiperdum* [55]. To further prove this finding, we extracted the DNA mass in the well as before and visualized it under AFM; indeed, we could observe catenated structures of several (but likely not all 10) maxicircles [Figs. 5(g) and 5(h)]. Thus, in light of these results we argue that at least some maxicircles are thread and weave along the periphery of the kDNA providing structural integrity and that they form a percolating subnetwork within the kDNA.

III. DISCUSSION

The kinetoplast DNA remains one of the most mysterious and fascinating structures in nature. Its biogenesis, self-assembly and replication are puzzling and still not fully understood. To address some of the open questions in this field we performed atomic force microscopy (AFM) on *C. fasciculata* kDNA samples that had been partially digested by restriction enzymes. We specifically identified restriction enzymes that cut different fractions of the kDNA structure via deep sequencing and DNA assembly. More specifically, we chose BssHII having no targets, PstI-targeting maxicircles

and <4% of minicircles (in total around 6% of kDNA mass), EcoRI-targeting maxicircles and around 13% of minicircles (in total around 15% of kDNA mass), and BmrI cutting all, and only, minicircles in *C. fasciculata* kDNA [Figs. 1(a), 1(b), and 1(d)].

First, we proposed a method to obtain kDNAs that is suitable for AFM: it employs gel electrophoresis to clean samples from enzymes, BSA, and other small kDNA fragments. We argue that it could be used in the future as a simple way to purify kDNA and other samples containing catenated structures such as some DNA origami and large genome sized DNA networks for AFM [Fig. 1(c)]. We then measured the change in shape and size of these structures and observed that both EcoRI- and PstI-treated structures displayed a significant reduction in circularity, with the border of PstI- and EcoRI-treated samples appearing more irregular and "blebbing" than control samples. These results suggested that both maxicircles and minicircles play an important role in kDNA border integrity (Fig. 2).

We then reported a marked change in size of PstI-treated kDNA samples, with a diameter reduced 1.5-fold when adsorbed on mica with respect to the control sample (Fig. 3). Intriguingly, size change was not detected via confocal microscopy in the bulk [22], i.e., when kDNA was not adsorbed on a surface. Additionally, we did not observe any significant shrinking in EcoRI-treated samples, and we rationalized this finding via a simple scaling argument [see Eq. (4)], which predicts that less polymer mass in the kDNA network reduces the effective adsorption strength but that cleaving minicircles may decrease the network stiffness. These two parameters, kDNA mass and network stiffness, balance each other and both affect the average network extension in opposite ways.

We note that similar kDNA structures have been recently prepared and analyzed via confocal microscopy in a bulk solution by Yadav *et al.* [22]. They reported that the digested kDNAs did not appear to assume a different size or shape, yet they displayed a different dynamical relaxation timescale, which they measured by computing correlations of the anisotropy vector. The increasing internal relaxation timescale was attributed to a smaller internal kDNA connectivity, which rendered the networks floppier and hence slower to relax. In contrast with their findings, we do instead observe a dramatic change in size (1.5-fold reduction) of PstI-treated samples (lacking mainly maxicircles) and a significant reduction of circularity in PstI- and EcoRI-treated samples (lacking both maxicircles and 13% of minicircles). Yet, in line with their findings, our results suggest that the EcoRI-treated networks are floppier than the control ones and can stretch more on the mica.

Further, we found that the hubs' height is significantly reduced after EcoRI treatment, suggesting that minicircles are the main component of those structures. At the same time, we found a significant change in border shape after PstI. We thus argue that maxicircles may assume a specific spatial distribution within the network and find visual, qualitative evidence that at least some of them may thread and weave along the border, contributing to the structural scaffolding of the hubs [Fig. 5(a)–5(e)]. Finally, by treating kDNAs with BmrI we found evidence that maxicircles form a percolated interlinked sub-network [Fig. 5(f)].

Overall, our single-molecule AFM quantitative characterization of partially digested kDNA offer some insight into kDNA's unique structure. Despite this, more work is needed to exactly pinpoint the spatial distribution of maxicircles and different classes of minicircles, and to dissect how each component contributes to the kDNA material properties. In the future, we plan to analyze and quantitatively compare the kDNA from different parasites; for instance, there are forms of trypanosomes that no longer depend on kDNA function and have lost maxicircles but not minicircles; thus, it would be natural to look at kDNA structures extracted from these strains [18]. We hope that ultimately, our results will complement others to achieve a full understanding of the biogenesis and self-assembly of this fascinating and mysterious structure.

IV. METHODS

A. kDNA sequencing and bioinformatic analysis

1. DNA assembly

Kinetoplast DNA from *C. fasciculata* was purchased from Inspiralis at 100 ng/μl in TE buffer (10 mM Tris-HCl pH7.5, 1 mM EDTA).

The kDNA sample was sequenced at NovoGene. After Microbial Whole Genome Library preparation (350 bp), libraries were pooled and sequenced on Illumina sequencer. Pair-end reads (150 bp) were generated, and about 4.7 million reads passed the quality filter.

To optimize the minicircle detection and construction, *de novo* assembly was performed in KOMICS with increase kmer sizes [56]. Contigs that contained the CSB3 (GGGGTTGGTGT) or its reverse complement, with one allowed mismatch to capture sequence variations, were tested for circularity. Fragments of the published minicircle sequence were detected and were annealed manually for circularization and comparison with the known sequence of major minicircle type in CfC1 [47]. The circularized contigs were orientated to the same strand and aligned at their anchor region. The published annotated minicircle fragments were detected in the *de novo* assembled complete minicircles [57]. After assembly with small kmers, contigs homologous to *Leishmania braziliensis* maxicircle were extracted for manual examination by global mapping that allowed one mismatch, to select for the longest homologous contig with complete read coverage.

2. Relative abundance estimation

After minicircles of three *T. congolense* strains were assembled, the conserved regions was identified by visually examining aligned minicircles. Motifs homologous to *T. brucei* CSB1, 2, and 3 were recognized in both conserved areas [48]. Illumina reads were mapped to the assemblies using Bowtie 2 with the `--very-sensitive` option [58]. Subsequent IGV visualization revealed no region with low or no coverage [59]. The minicircle assemblies incorporated over 96% of kDNA reads. The completeness was confirmed by >98% mapped CSB3-containing reads and >97% CSB3-containing reads mapped with quality $\geqslant 10$. More specifically, we obtained 4 701 610 total reads, mapped 4 516 344 (96%) and a total of 494 007 CSB3-containing

reads, and mapped 489 034 (98%). The relative abundance of 18 unique minicircles was estimated from mean read depth calculated by SAMtools [49].

3. Minicircle annotation

C. fasciculata maxicircle was aligned to annotated *L. major* maxicircle and subsequently to unedited *L. major* maxicircle genes for annotation. The annotation was confirmed by aligning transcriptomic data from *in vitro* adherent and swimming form of *C. fasciculata* and infected mosquito hindguts [51]. Using the unedited *C. fasciculata* maxicircle genes as a reference, T-aligner performed T-masked mapping to detect consistently edited encrypted genes that were used in subsequent edited gene prediction and minicircle annotation [52]. The published A6- and uS12m-edited mRNAs [57] as well as predicted edited ND7 and COXII mRNAs [51] were validated by alignment of the transcriptomic data with Bowtie2 [58]. Guide RNA prediction was achieved using a custom version of the kDNA annotation package [48]. Restriction enzyme cutting sites on *C. fasciculata* minicircles and maxicircle were predicted for enzymes available from New England Biolabs (NEB) using a custom python script to facilitate enzyme choice.

B. kDNA digestion

To avoid shearing of kDNA, we used 200 µl large orifice tips. In the Supplemental Material [50] we show that even after repeated pipetting of the same sample, our handling does not generate any shearing and breakage of the kDNA structure. For restriction digestion with EcoRI, PstI, and BssHII (all from NEB), 1 µl of enzyme (10 units) was used to digest 1 µg of kDNA in 1× rCutsmart buffer, overnight at 37 °C. The BssHII restriction digestion sample was incubated at 50 °C for 2 hours prior to overnight incubation at 37 °C. The samples were then run on a gel and recovered from the wells, as described above. After recovery, the samples were adsorbed on freshly cleaved mica, dip washed in ultra-pure water for 1 minute, and gently air dried in ultrapure nitrogen stream.

C. AFM images acquisition and analysis

The AFM images were recorded in Bruker JPK NanoWizard 4XP using SNL-10 probes. To maintain uniformity in comparing the structural changes, we traced only the circular kDNA structures and recorded the topographs at high resolution (2000 pixels×2000 pixels). The AFM topographs were postprocessed in the JPK data-processing software and converted into TIF files. We then used ImageJ to manually compute the area of each kDNA, distance between hubs, and pore size using morphological segmentation via MorphoLibJ [60] as previously described [36]. The heights of the hubs in Fig. 4(e) were quantified using Gwyddion software. For each AFM image, individual height profiles were generated for a minimum of 50 hubs, and the peak maxima for each hub were recorded to calculate the average height in nm.

To obtain the average height of the whole kDNA, we performed an analysis using MountainsSPIP software. First, the AFM images were preprocessed using the least square plane (LSPL) subtraction function to flatten any long-range slope in the AFM images. Subsequently, a line-by-line leveling process was applied by subtracting the least square polynomial and mean values to ensure straightness and align each scan line onto a uniform flat surface within the image. The resulting flat images and data points were then used to generate a histogram of the pixel height distribution (see the Supplemental Material [50]). Within the histogram, two prominent peaks corresponding to the mica surface and kDNA structures (adsorbed DNA) were identified. We then calculated the average height of the kDNA structures by taking the difference between the two maxima of the two peaks.

D. Agarose gel electrophoresis

We prepared 0.5 µg of kDNA with 0.5 μl of restriction enzymes (BssHII, Pst1, EcoRI) in 1× rCutsmart buffer and incubated overnight at 37 °C. The BssHII sample was incubated at 50 °C for 2 hours before the overnight incubation, as per NEB recommendations. A 0.8% agarose gel was cast in 1× TAE buffer, and 25 µl of restriction digested kDNA samples (plus a control sample) were prepared in 1× loading dye and run for 5 hours at 50 V (about 5 V/cm). The gel was stained with SYBR gold and imaged in a Gel Doc imaging system.

The minicircle assembly is deposited on GenBank OR687467–OR687484. The annotated maxicircle sequences are deposted on Figshare [61], along with all minicircle sequences, information on gRNAs, and editing site coverage by gRNAs.

ACKNOWLEDGMENTS

D.M. thanks the Royal Society for support through a University Research Fellowship. This project has received funding from the European Research Council (ERC) under the European Union's Horizon 2020 research and innovation program (grant agreement No 947918, TAP). The authors also acknowledge the contribution of the COST Action Eutopia, CA17139. Z.C. was supported by an EASTBIO PhD studentship from the UK Biotechnology and Biological Sciences Research Council (BBSRC). We thank Laura Charlton for her help with AFM.

[1] L. P. Simpson, Morphogenesis and the function of the kinetoplast in "Leishmania", Atlas Symp. Biota Amazonica (Pathologia) **6**, 231 (1967).

[2] M. Laurent and M. Steinert, Electron microscopy of kinetoplastic DNA from *Trypanosoma mega*, Proc. Natl. Acad. Sci. USA **66**, 419 (1970).

[3] J. Shlomai and A. Zadok, Reversible decatenation of kinetoplast DNA by a DNA topoisomerase from trypanosomatids, Nucleic Acids Res. **11**, 4019 (1983).

[4] D. L. Pérez-Morga and P. T. Englund, The attachment of minicircles to kinetoplast DNA networks during replication, Cell **74**, 703 (1993).

[5] J. Shlomai, The assembly of kinetoplast DNA, Parasitol. Today **10**, 341 (1994).

[6] J. C. Morris, M. E. Drew, M. M. Klingbeil, S. A. Motyka, T. T. Saxowsky, Z. Wang, and P. T. Englund, Replication of kinetoplast DNA: An update for the new millennium, Int. J. Parasitol. **31**, 453 (2001).

[7] J. Lukeš, D. Guilbride, and J. Votýpka, Kinetoplast DNA network: Evolution of an improbable structure, Eukaryot. Cell **1**, 495 (2002).

[8] L. Simpson, O. H. Thiemann, N. J. Savill, J. D. Alfonzo, and D. A. Maslov, Evolution of RNA editing in trypanosome mitochondria, Proc. Natl. Acad. Sci. USA **97**, 6986 (2000).

[9] S. Hajduk and T. Ochsenreiter, RNA Biology **7**, 229 (2010).

[10] B. Liu, Y. Liu, S. A. Motyka, E. E. C. Agbo, and P. T. Englund, Fellowship of the rings: The replication of kinetoplast DNA, Trends Parasitol. **21**, 363 (2005).

[11] M. M. Klingbeil, M. E. Drew, Y. Liu, J. C. Morris, S. A. Motyka, T. T. Saxowsky, Z. Wang, and P. T. Englund, Unlocking the secrets of trypanosome kinetoplast DNA network replication, Protist **152**, 255 (2001).

[12] A. Hoffmann, S. Käser, M. Jakob, S. Amodeo, C. Peitsch, J. Týc, S. Vaughan, B. Zuber, A. Schneider, and T. Ochsenreiter, Molecular model of the mitochondrial genome segregation machinery in *Trypanosoma brucei*, Proc. Nat. Acad. Sci. USA **115**, E1809 (2018).

[13] A. Schnaufer, Evolution of dyskinetoplastic trypanosomes: How, and how often? Trends Parasitol. **26**, 557 (2010).

[14] A. Kalichava and T. Ochsenreiter, Ultrastructure expansion microscopy in *Trypanosoma brucei*, Open Biol. **11**, 210132 (2021).

[15] S. Amodeo, A. Kalichava, A. Fradera-Sola, E. Bertiaux-Lequoy, P. Guichard, F. Butter, and T. Ochsenreiter, Characterization of the novel mitochondrial genome segregation factor TAP110 in *Trypanosoma brucei*, J. Cell Sci. **134**, jcs254300 (2021).

[16] S. Amodeo, I. Bregy, and T. Ochsenreiter, Mitochondrial genome maintenance–the kinetoplast story, FEMS Microbiol. Rev. **47**, fuac047 (2022).

[17] J. Lukeš, H. Hashimi, and A. Zíková, Unexplained complexity of the mitochondrial genome and transcriptome in kinetoplastid flagellates, Curr. Genet. **48**, 277 (2005).

[18] A. Schnaufer, G. J. Domingo, and K. Stuart, Natural and induced dyskinetoplastic trypanosomatids: How to live without mitochondrial DNA, Int. J. Parasitol. **32**, 1071 (2002).

[19] B. W. Soh, A. Khorshid, D. Al Sulaiman, and P. S. Doyle, Ionic effects on the equilibrium conformation of catenated DNA networks, Macromolecules **53**, 8502 (2020).

[20] B. W. Soh and P. S. Doyle, Equilibrium conformation of catenated DNA networks in slitlike confinement, ACS Macro Lett. **10**, 880 (2021).

[21] A. R. Klotz, B. W. Soh, and P. S. Doyle, Equilibrium structure and deformation response of 2D kinetoplast sheets, Proc. Natl. Acad. Sci. USA **117**, 121 (2020).

[22] I. Yadav, D. Al Sulaiman, and P. S. Doyle, Tuning the topology of a two-dimensional catenated DNA network, Phys. Rev. Res. **5**, 013141 (2023).

[23] A. Y. Grosberg, Human bloodsucking parasite in service of materials science, Proc. Natl. Acad. Sci. USA **117**, 18 (2020).

[24] L. Tubiana, F. Ferrari, and E. Orlandini, Circular polycatenanes: Supramolecular structures with topologically tunable properties, Phys. Rev. Lett. **129**, 227801 (2022).

[25] T. A. Vilgis and M. Otto, Elasticity of entangled polymer loops: Olympic gels, Phys. Rev. E **56**, R1314(R) (1997).

[26] Q. Wu, P. M. Rauscher, X. Lang, R. J. Wojtecki, J. J. De Pablo, M. J. Hore, and S. J. Rowan, Poly[*n*]catenanes: Synthesis of molecular interlocked chains, Science **358**, 1434 (2017).

[27] J. Fischer, M. Lang, and J.-U. Sommer, The formation and structure of Olympic gels, J. Chem. Phys. **143**, 243114 (2015).

[28] M. Lang, J. Fischer, M. Werner, and J. U. Sommer, Swelling of Olympic gels, Phys. Rev. Lett. **112**, 238001 (2014).

[29] S. Igram, K. C. Millett, and E. Panagiotou, Resolving critical degrees of entanglement in Olympic ring systems, J. Knot Theory Ramifications **25**, 1650081 (2016).

[30] Y. Diao, K. Hinson, R. Kaplan, M. Vazquez, and J. Arsuaga, The effects of density on the topological structure of the mitochondrial DNA from trypanosomes, J. Math. Biol. **64**, 1087 (2012).

[31] D. Michieletto, D. Marenduzzo, E. Orlandini, G. Alexander, and M. Turner, Dynamics of self-threading ring polymers in a gel, Soft Matter **10**, 5936 (2014).

[32] Y. S. Kim, B. Kundukad, A. Allahverdi, L. Nordensköld, P. S. Doyle, and J. R. Van Der Maarel, Gelation of the genome by topoisomerase II targeting anticancer agents, Soft Matter **9**, 1656 (2013).

[33] B. A. Krajina, A. Zhu, S. C. Heilshorn, and A. J. Spakowitz, Active DNA Olympic hydrogels driven by topoisomerase activity, Phys. Rev. Lett. **121**, 148001 (2018).

[34] J. Chen, C. A. Rauch, J. H. White, P. T. Englund, and N. Cozzarelli, The topology of the kinetoplast DNA network, Cell **80**, 61 (1995).

[35] L. Ibrahim, P. Liu, M. Klingbeil, Y. Diao, and J. Arsuaga, Estimating properties of kinetoplast DNA by fragmentation reactions, J. Phys. A: Math. Theor. **52**, 034001 (2019).

[36] P. He, A. J. Katan, L. Tubiana, C. Dekker, and D. Michieletto, Single-molecule structure and topology of kinetoplast DNA networks, Phys. Rev. X **13**, 021010 (2023).

[37] M. A. Ubertini and A. Rosa, Topological analysis and recovery of entanglements in polymer melts, Macromolecules **56**, 3354 (2023).

[38] G. Palombo, S. Weir, D. Michieletto, and Y. A. G. Fosado, Topological elasticity in physical gels with limited valence, arXiv:2308.09689.

[39] S. Datta, Y. Kato, S. Higashiharaguchi, K. Aratsu, A. Isobe, T. Saito, D. D. Prabhu, Y. Kitamoto, M. J. Hollamby, A. J. Smith, R. Dagleish, N. Mahmoudi, L. Pesce, C. Perego, G. M. Pavan, and S. Yagai, Self-assembled poly-catenanes from supramolecular toroidal building blocks, Nature **583**, 400 (2020).

[40] A. Peil, P. Zhan, and N. Liu, DNA Origami Catenanes Templated by Gold Nanoparticles, Small **16**, 1 (2020).

[41] D. C. Barker, The ultrastructure of kinetoplast DNA with particular reference to the interpretation of dark field electron microscopy images of isolated, purified networks, Micron (1969) **11**, 21 (1980).

[42] M. L. Ferguson, A. F. Torri, D. Pérez-Morga, D. C. Ward, and P. T. Englund, Kinetoplast DNA replication: Mechanistic differences between *Trypanosoma brucei* and *Crithidia fasciculata*, J. Cell Biol. **126**, 631 (1994).

[43] D. P. Cavalcanti, D. L. Gonçalves, L. T. Costa, and W. de Souza, The structure of the kinetoplast DNA network of *Crithidia fasciculata* revealed by atomic force microscopy, Micron **42**, 553 (2011).

[44] N. Yaffe, D. Rotem, A. Soni, D. Porath, and J. Shlomai, Direct monitoring of the stepwise condensation of kinetoplast DNA networks, Sci. Rep. **11**, 1501 (2021).

[45] J. Ragotskie, N. Morrison, C. Stackhouse, R. C. Blair, and A. R. Klotz, The effect of the kinetoplast edge loop on network percolation, J. Polym. Sci. **n/a**.

[46] M. Geerts, A. Schnaufer, and F. Van den Broeck, rKOMICS: an R package for processing mitochondrial minicircle assemblies in population-scale genome projects, BMC Bioinformatics **22**, 468 (2021).

[47] H. Sugisaki and D. S. Ray, DNA sequence of Crithidia fasciculata kinetoplast minicircles, Molecular biochem. parasitology **23**, 253 (1987).

[48] S. Cooper, E. S. Wadsworth, T. Ochsenreiter, A. Ivens, N. J. Savill, and A. Schnaufer, Nucleic Acids Res. **47**, 11304 (2019).

[49] H. Li, B. Handsaker, A. Wysoker, T. Fennell, J. Ruan, N. Homer, G. Marth, G. Abecasis, and R. Durbin, Bioinformatics (Oxford, England) **25**, 2078 (2009).

[50] See Supplemental Material at http://link.aps.org/supplemental/10.1103/PRXLife.2.013009 for additional description of the methods, AFM images and aimage analysis.

[51] J. N. Filosa, C. T. Berry, G. Ruthel, S. M. Beverley, W. C. Warren, C. Tomlinson, P. J. Myler, E. A. Dudkin, M. L. Povelones, and M. Povelones, PLoS Neglected Tropical Diseases **13**, 1 (2019).

[52] E. S. Gerasimov, A. A. Gasparyan, I. Kaurov, B. Tichý, M. D. Logacheva, A. A. Kolesnikov, J. Lukeš, V. Yurchenko, S. L. Zimmer, and P. Flegontov, Nucleic Acids Res. **46**, 765 (2018).

[53] P.-G. de Gennes, *Scaling Concepts in Polymer Physics* (Cornell University Press, Ithaca, NY, 1979).

[54] E. Gluenz, M. L. Povelones, P. T. Englund, and K. Gull, The kinetoplast duplication cycle in *Trypanosoma brucei* is orchestrated by cytoskeleton-mediated cell morphogenesis, Mol. Cell. Biol. **31**, 1012 (2011).

[55] T. A. Shapiro, Kinetoplast DNA maxicircles: Networks within networks, Proc. Natl. Acad. Sci. USA **90**, 7809 (1993).

[56] F. Van den Broeck, N. J. Savill, H. Imamura, M. Sanders, I. Maes, S. Cooper, D. Mateus, M. Jara, V. Adaui, J. Arevalo, A. Llanos-Cuentas, L. Garcia, E. Cupolillo, M. Miles, M. Berriman, A. Schnaufer, J. A. Cotton, and J. C. Dujardin, Ecological divergence and hybridization of Neotropical Leishmania parasites, Proc. Natl. Acad. Sci. USA **117**, 25159 (2020).

[57] S. Yasuhira and L. Simpson, Minicircle-encoded guide RNAs from Crithidia fasciculata, RNA **1**, 634 (1995).

[58] B. Langmead and S. L. Salzberg, Fast gapped-read alignment with Bowtie2, Nat. Methods **9**, 357 (2012).

[59] J. T. Robinson, H. Thorvaldsdóttir, W. Winckler, M. Guttman, E. S. Lander, G. Getz, and J. P. Mesirov, Integrative genomics viewer, Nat. Biotech. **29**, 24 (2011).

[60] D. Legland, I. Arganda-Carreras, and P. Andrey, MorphoLibJ: Integrated library and plugins for mathematical morphology with ImageJ, Bioinformatics **32**, 3532 (2016).

[61] https://10.6084/m9.figshare.24968601.